X-band Polarimetric Radar Rainfall Measurements in Keys Area Microphysics Project

EMMANOUIL N. ANAGNOSTOU

Department of Civil and Environmental Engineering, University of Connecticut, Storrs, Connecticut

MIRCEA GRECU

Goddard Earth Sciences and Technology Center, University of Maryland, Baltimore County, Baltimore, and NASA Goddard Space Flight Center, Greenbelt, Maryland

MARIOS N. ANAGNOSTOU

Department of Civil and Environmental Engineering, University of Connecticut, Storrs, Connecticut

(Manuscript received 11 November 2003, in final form 12 January 2005)

ABSTRACT

The Keys Area Microphysics Project (KAMP), conducted as part of NASA's Fourth Convective and Moisture Experiment (CAMEX-4) in the lower Keys area, deployed a number of ground radars and four arrays of rain gauge and disdrometer clusters. Among the various instruments is an X-band dual-polarization Doppler radar on wheels (XPOL), contributed by the University of Connecticut. XPOL was used to retrieve rainfall rate and raindrop size distribution (DSD) parameters to be used in support of KAMP science objectives. This paper presents the XPOL measurements in KAMP and the algorithm developed for attenuation correction and estimation of DSD model parameters. XPOL observations include the horizontal polarization reflectivity Z_H, differential reflectivity $Z_{\rm DR}$, and differential phase shift $\Phi_{\rm DP}$. Here, Z_H and $Z_{\rm DR}$ were determined to be positively biased by 3 and 0.3 dB, respectively. A technique was also applied to filter noise and correct for potential phase folding in $\Phi_{\rm DP}$ profiles. The XPOL attenuation correction uses parameterizations that relate the path-integrated specific (differential) attenuation along a radar ray to the filtered-$\Phi_{\rm DP}$ (specific attenuation) profile. Attenuation-corrected Z_H and specific differential phase shift (derived from filtered $\Phi_{\rm DP}$ profiles) data are then used to derive two parameters of the normalized gamma DSD model, that is, intercept (N_w) and mean drop diameter (D_0). The third parameter (shape parameter μ) is calculated using a constrained μ–Λ relationship derived from the measured raindrop spectra. The XPOL attenuation correction is evaluated using coincidental nonattenuated reflectivity fields from the Key West Weather Surveillance Radar-1988 Doppler (WSR-88D), while the DSD parameter retrievals are statistically assessed using DSD parameters calculated from the measured raindrop spectra. Statistics show that XPOL DSD parameter estimation is consistent with independent observations. XPOL estimates of water content and N_w are also shown to be consistent with corresponding retrievals from matched ER-2 Doppler radar (EDOP) profiling observations from the 19 September airborne campaign. Results shown in this paper strengthen the applicability of X-band dual-polarization high resolution observations in cloud modeling and precipitation remote sensing studies.

1. Introduction

The primary objective of the Keys Area Microphysics Project (KAMP), conducted during National Aeronautics and Space Administration's (NASA) fourth Convective and Moisture Experiment (CAMEX) campaign in the southern Keys area was to facilitate validation of cloud-resolving and radiative models in tropical oceanic regime. Simulated profiles of cloud and precipitation parameters and corresponding radiative transfer properties are used to build physically based algorithms for precipitation retrieval from satellite passive (radiometers) and active [Tropical Rainfall Measuring Mission (TRMM) precipitation radar] microwave observations (Smith et al. 1994; Kummerow and

Corresponding author address: Emmanouil N. Anagnostou, Dept. of Civil and Environmental Engineering, University of Connecticut, 261 Glenbrook Road, Storrs, CT 06269.
E-mail: manos@engr.uconn.edu

Giglio 1994; Olson et al. 1996). This is currently the most popular approach in satellite precipitation profile retrieval as it represents a good trade-off between mathematical rigors, flexibility in describing real-life situations, and computational efficiency. Nevertheless, there are issues that limit the accuracy of these retrievals. These issues arise mainly in the cloud model realism and our incomplete knowledge about the microphysical structure of oceanic storms and its relation to radiometric measurements. Improvement in these two aspects would lead to more accurate estimates and a better understanding of the underlying processes. This is critical, since space-based sensors are the main realistic tool for obtaining quantitative assessment of tropical systems over regions beyond the quantitative range of ground weather radars.

An array of ground based research instruments were deployed in KAMP to provide comprehensive cloud and precipitation observations. Continuous monitoring of rainfall patterns was based on a network of five ground weather radars, which include 1) two NASA radars, the C-band single polarization Doppler radar [referred to as Tropical Ocean Global Atmosphere (TOGA)] and the newly built dual-polarization Doppler radar (referred to as NPOL); 2) the operational National Weather Service Weather Surveillance Radar-1988 Doppler (WSR-88D) in Key West (referred to as 88D); 3) the Texas A&M mobile C-band single polarization Doppler radar (referred to as S-R); and (4) a mobile X-band dual-polarization weather radar (referred to as XPOL) contributed by the University of Connecticut. In addition to the weather radar observations, in situ networks of rain gauges and disdrometers deployed by NASA, and a vertical integrated profiling system (MIPS) contributed by the University of Alabama in Huntsville have provided point rainfall rate and drop size distribution measurements. A main objective of KAMP is to derive, based on combined dual-Doppler and dual-polarization radar measurements, accurate estimates of surface rainfall and wind fields and to improve our knowledge on rain microphysics at fine spatial and temporal scales. These estimates would facilitate the development of improved cloud model profiles and provide the microphysical information needed in radiative transfer calculations. This paper describes the XPOL observations in KAMP, and the development of an algorithm for estimation of precipitation water content, the mean raindrop diameter, and the intercept coefficient of the normalized gamma drop size distribution model.

Rainfall estimation from polarimetric radar measurements is a problem studied extensively in the past two decades (Jameson 1991; Ryzhkov and Zrnić 1995; Zrnić and Ryzhkov 1996; Blackman and Illingworth 1997; Vivekanandan et al. 1999). A primary focus has been in the retrieval of rain rates using combination of horizontal polarization reflectivity (Z_H), differential reflectivity (Z_{DR}) and specific differential phase shift (K_{DP}) parameters measured by nonattenuating wavelength (S band) radars. Recent studies by Bringi et al. (2002) and Brandes et al. (2003) have shown that simultaneous use of the above polarimetric parameters at S band can be used to derive raindrop size distribution (DSD) parameters, thereby estimating other rainfall parameters such as rainfall rate and water content. Although, S-band frequency has the advantage of being less sensitive to rain-path attenuation compared to higher frequencies (e.g., C and X bands), a disadvantage has been the lower sensitivity of the differential measurements (primarily K_{DP}) to rainfall rate. Consequently, in cases of moderate to low rainfall rates definitive estimates of DSD are possible through averaging along a radar ray, which impacts the resolution of precipitation estimates. Bringi et al. (2002) described such a retrieval designed to deal with low rainfall intensities. Since the sensitivity of differential phase (Φ_{DP}) measurement to the raindrop size is proportional to the radar frequency, at higher frequencies these limiting values are lowered by a factor of up to 3 (e.g., at X band). Consequently, the use of shorter wavelengths should allow more detailed quantitative measurement of light to moderate rainfall rates (Matrosov et al. 2005, 2002; Anagnostou et al. 2004; May et al. 1999; Jameson 1991). However, the Z_H and Z_{DR} measurements at higher frequencies are sensitive to rain-path attenuation, while attenuation is not an issue for the K_{DP} parameter unless there is complete signal loss due to attenuation (i.e., signal drops below a minimum detection threshold). A common approach to attenuation correction for short wavelength radar data has been the use of K_{DP} (derived from Φ_{DP} ray profiles) related through power-law functions to specific (A_H, in dB km^{-1}) and differential (A_{DP}, in dB km^{-1}) attenuation parameters.

There are two main complications in using K_{DP} measurements for correcting attenuated reflectivity and differential reflectivity profiles. The first is the presence of δ effect in Φ_{DP} measurements when there is significant concentration of large drops causing a resonance effect (Testud et al. 2000). The second is the dependence of the A_H (A_{DP})–K_{DP} functions on the raindrop oblateness–size relationship. This dependence can significantly affect attenuation correction as the raindrops' oblateness–size relation may vary because of drop oscillations and drop canting, which tend to bias the axis ratio from the equilibrium condition. The δ effect, which appears in the data as a rapid increase/decrease

(i.e., a bump that would stand above the random Φ_{DP} noise variations) in the Φ_{DP} profile, causes errors in the derivation of K_{DP} values thus affecting the estimation accuracy of A_H and A_{DP} profiles (Testud et al. 2000; Matrosov et al. 2002). Zrnić et al. (2000) and Keenan et al. (2001) have studied the sensitivity of attenuating frequency (C band) radar parameters on the form of raindrop axial ratio exemplifying its effect of rainfall estimation.

Currently, research on the use of dual-polarization radar rainfall measurements at X band has been limited to a few theoretical (Jameson 1994, 1991; Chandrasekar and Bringi 1988a,b; Chandrasekar et al. 1990) and experimental studies (Matrosov et al. 1999, 2002; Anagnostou et al. 2004). Both Matrosov et al. and Anagnostou et al. studies used experimental data to conduct a quantitative error analysis of various multi- and single-parameter rain estimators. They concluded that the estimator that uses attenuation-corrected Z_H and Z_{DR} profiles jointly with δ-corrected K_{DP} profile provides the least standard error in rain rates compared to other single parameter estimators. In addition to rainfall estimation, Anagnostou et al. (2004) described a way of retrieving the intercept parameter of the normalized gamma DSD model (N_w), which was shown to be consistent with corresponding N_w values derived from coincidental 3-min-averaged DSD spectra measurements. A commonality to be drawn is that the raindrop oblateness–size variability significantly affects attenuation correction and rain retrieval relationships, which is an aspect that should be accounted for in the retrieval.

The current research, which builds upon our previous work (Anagnostou et al. 2004), is focused on issues that remained unexplored in previous studies. Specifically, some of the previous experimental studies (Matrosov et al. 1999; Anagnostou et al. 2004) were based exclusively on radar observations of stratiform, low intensity rain. As some of the difficulties associated with X-band polarimetric radar precipitation estimation exacerbate with the rain-rate increase, a detailed investigation of X-band polarimetric radar estimation of high intensity, highly variable, rainfall is needed. Matrosov et al. (2002) investigated X-band polarimetric retrievals of convective precipitation, but noted a remarkably small δ effect. That is something quite rare and probably of consequence of relatively small horizontal rain variability. However, in practice, especially in tropical or subtropical environments, large horizontal rain variability, and, consequently, δ effect are likely to occur. In this respect, the data collected in KAMP represent an excellent opportunity, as they are characterized by a large variety of storms featuring both stratiform and convective precipitation. The microphysical analysis of these storms is the subject of a different study. In the current study, we are concerned only with the accuracy of various precipitation-related variable retrievals.

The first step of our approach is to determine potential offsets in XPOL Z_H and Z_{DR} measurements and derive Φ_{DP} profile filtered from noise and potential phase folding and δ effects (hereafter named Ψ_{DP}). Offset-adjusted Z_H and Z_{DR} profiles are corrected for attenuation using power-law functions relating A_H (A_{DP}) to Ψ_{DP} profiles. The attenuation-corrected Z_H and Z_{DR} and K_{DP} (derived from Ψ_{DP} profile) ray profiles are used to retrieve profiles of N_w and mean drop diameter (D_0) DSD parameters. Using a constrained relation between the shape and slope parameters of gamma DSD model along with the retrieved N_w and D_0 values we estimate all three parameters of gamma DSD for discrete space intervals along a radar ray. Rainfall rate, water content, and other parameters are then derivable from the retrieved DSD parameters. Coincidental and closely matched radar reflectivity measurements from the nonattenuated (S band) Key West WSR-88D are used to evaluate the attenuation correction procedure. The XPOL-retrieved DSD parameters are then compared against corresponding parameters derived from in situ DSD spectra measurements to determine the physical consistency of the retrieval. The high-resolution three-dimensional reflectivity fields and DSD products derived from XPOL observations in KAMP can facilitate evaluation of cloud model simulations and airborne or satellite radar/radiometer oceanic rainfall retrievals.

The paper is organized in six sections. Description of the data used in this study is provided in section 2. In section 3 we provide background information on X-band polarimetric radar parameters, while in section 4 we present the XPOL retrieval algorithms. In section 5 we present case studies used to assess the algorithm through comparison with independent observations, and in section 6 we provide conclusions.

2. Experimental data

a. Overview

As discussed in the introduction, KAMP project deployed among other instruments an X-band polarimetric radar on wheels contributed by the University of Connecticut. The XPOL radar specs are summarized in Table 1. Figure 1 shows the XPOL location in reference to the other instruments deployed in KAMP. The radar was located on a small hill (~15 m above sea level) at Cudjoe Key, which was approximately 22 km from 88D and NPOL radars, 10 km from TOGA radar, 26 km from S-R radar, and 8 km from MIPS (an integrated

TABLE 1. Specifications of the mobile XPOL scanning radar.

Transmitter system	2.98-cm radar wavelength, 50-kW peak transmit power, and selectable pulse length (38–150-m resolution volumes).
Polarization diversity	Simultaneous transmission of signal at horizontal and vertical polarization.
Antenna system	0.95°, 3-dB beamwidth (8.5-ft antenna), and a maximum of 30° s^{-1} azimuth rotation. During operation antenna center is about 8 ft from the ground.
Antenna control system	Plan position indicator, range–height indicator, and survey scan modes. Programmable azimuth and elevation boundaries and step angles and rates. Solar calibration mode.
Radar measurables	Horizontal and vertical polarization reflectivity, Doppler velocities, spectral width, differential phase shift, and specific differential phase shift.
Radar calibration	Use of a signal generator to calibrate the antenna gain. Use of solar calibration and GPS for exact radar positioning.
Mobile platform	Radar system mounted on a flatbed truck with radar operations cabin, a hydraulic leveling system, and a diesel power generator.

vertical profiling system from the University of Alabama in Huntsville). XPOL was operated on a storm event basis in a hybrid volume-scanning, sector-scanning, and range–height indicator mode with elevations ranging from 0.2° to 50°. Because of the use of simultaneous horizontal and vertical polarization transmission the antenna scanning rate was set to higher rotation speeds (~10° s^{-1}) providing faster updates of full scanning cycles (3–5 min). In Fig. 2 we summarize the data record of XPOL measurements in KAMP.

There were four dual–rain gauge/disdrometer clusters located within 30 km of XPOL range. The disdrometers are Joss–Waldvogel (JW) type, which is a long-time community standard (Joss and Waldvogel 1967). The DSD spectral measurements had been quality controlled by NASA TRMM office and compared against rainfall rates derived from the coincidental clusters of double tipping-bucket (0.25 mm) rain gauges available at each disdrometer site (Tokay et al. 2003). Over 4000 quality-controlled 3-min-averaged raindrop spectra associated with rain rates greater than 0.5 mm h^{-1} were selected from the available DSD data.

b. XPOL calibration

Given that XPOL is a fairly new system basic measurement noise tests were performed during and after completion of the experiment to evaluate the system performance. To determine the measurement noise statistics we used multiple fixed-antenna samples (taking 100 bins per sample) during low precipitation intensity periods. The statistics evaluated from those samples showed noise standard deviations in the range of 0.15–0.25 (mode at ~0.2) dBZ for Z_H, 0.22–0.46 (mode at ~0.3) dB for Z_{DR}, and 1°–4° (mode at 1.6°) for Φ_{DP}. To determine the Z_H calibration bias we compared against coincident reflectivity observations from the Key West 88D (KEYW). The 88D calibration was assessed against the Tropical Rainfall Measuring Mission pre-

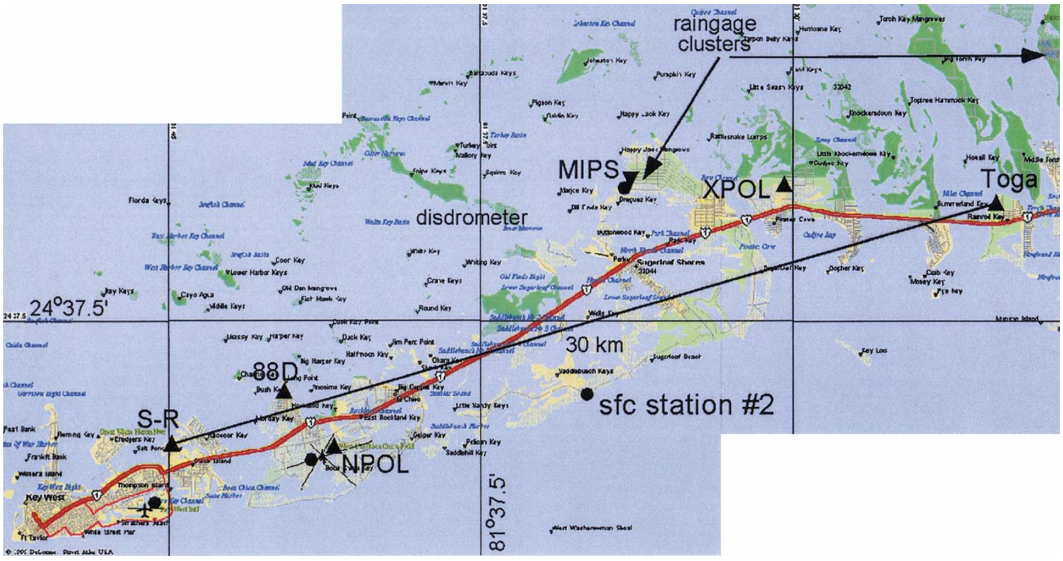

FIG. 1. KAMP ground instrumentation locations.

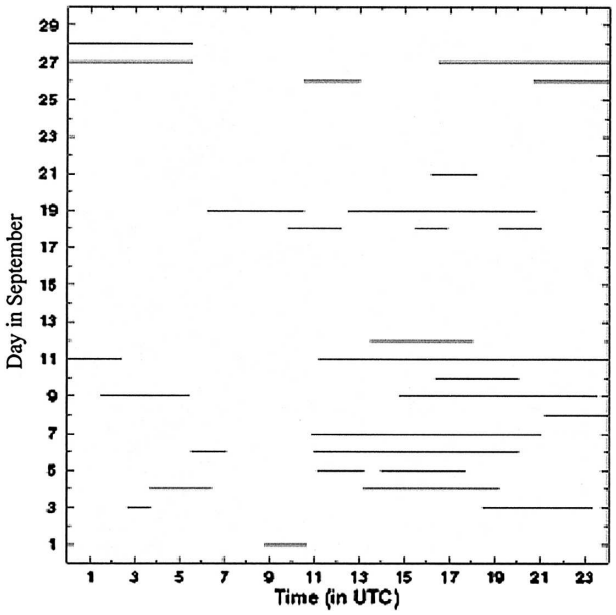

FIG. 2. The XPOL measurement record in KAMP.

cipitation radar (PR) on the basis of the Anagnostou et al. (2001) algorithm and found to be on average 1 dB below PR. Comparison statistics between attenuation-corrected XPOL and 88D matched reflectivity values showed that XPOL has a 3.5-dB positive bias with respect to the 88D. Walters et al. (2004) indicated a positive bias of ~2.5 dB comparing an XPOL reflectivity profile to a corresponding profile measured by MIPS (8-km range from XPOL) for a stratiform precipitation case. It is noted that the MIPS reflectivity values are calibrated to DSD spectra measured by a JW disdrometer located at the profiler site (see Fig. 1 of Walters et al. 2004). Our collective evidence based on XPOL comparisons with MIPS and 88D is a 3-dB positive bias for XPOL. The Z_{DR} calibration was determined from measurements collected with vertically (90°) pointing and rotating antenna in light precipitation. Those data indicated a positive bias of ~0.3 dB. Finally, we have devised a scheme for correcting differential phase (Φ_{DP}) measurements from range folding, and implemented Hubbert and Bringi (1995) filter to remove noise from the data. Visual inspection on a number of filtered Φ_{DP} ray profiles showed that the algorithm works well; that is, the folding was removed and variability due to noise was smoothed out. From the filtered Φ_{DP} profiles (named Ψ_{DP} profile) we can now readily derive K_{DP} values.

3. Background

In this section we summarize the basic physical relationships between radar parameters and raindrop spectra. The parameters considered are the X-band measured (i.e., attenuated) reflectivity at H and V polarizations, $Z_{a\mathrm{H}}$ and $Z_{a\mathrm{V}}$ (in mm^6 m^{-3}) from which we derive the attenuated differential reflectivity, $Z_{a\mathrm{DR}} = Z_{a\mathrm{H}}/Z_{a\mathrm{V}}$ (in dB); the differential phase shift, Φ_{DP} (in deg) from which we derive the specific differential phase shift by taking its gradient along a radar ray, K_{DP} (deg km^{-1}). The above measurements can be related to equivalent (nonattenuated) radar parameters as follows:

$$Z_{a\mathrm{H}}(r) = Z_{e\mathrm{H}}(r) \times 10^{-0.2\int_0^r A_{\mathrm{H}}(s)\,ds}, \tag{1}$$

$$Z_{a\mathrm{DR}}(r) = Z_{\mathrm{DR}}(r) \times 10^{-0.2\int_0^r A_{\mathrm{DP}}(s)\,ds}, \tag{2}$$

$$\Phi_{\mathrm{DP}}(r) = \delta(r) + 2\int_0^r K_{\mathrm{DP}}(s)\,ds, \tag{3}$$

where $Z_{e\mathrm{H}}$ and Z_{DR} are the equivalent (nonattenuated) radar reflectivity and differential reflectivity parameters, while A_H and A_{DP} (dB km^{-1}) are the specific attenuation and differential attenuation parameters, respectively. These parameters are related to the hydrometeor size distribution (DSD) within a radar sampling volume through the following integral equations (Bringi and Chandrasekar 2002):

$$Z_{e\mathrm{H,V}} = \frac{\lambda^4}{\pi^5}\left|\frac{m^2+2}{m^2-1}\right|\int_0^{D_{\max}} \sigma_{b\mathrm{H,V}}(D_e)N(D_e)\,dD_e, \tag{4}$$

$$A_{\mathrm{H,V}} = 2\lambda\int_0^{D_{\max}} \mathrm{Im}[f_{\mathrm{H,V}}(K_1,K_1;D_e)]N(D_e)\,dD_e, \tag{5}$$

$$K_{\mathrm{DP}} = \lambda\int \{\mathrm{Re}[f_{\mathrm{H}}(K_1,K_1;D_e)] - \mathrm{Re}[f_V(K_1,K_1;D_e)]\}N(D_e)\,dD_e \tag{6}$$

$$\delta = \arg\left[\int_0^{D_{\max}} f_{\mathrm{H}}(K_1,-K_1;D_e)\,f_{\mathrm{V}}{}^*(K_1,-K_1;D_e)N(D_e)\,dD_e\right], \tag{7}$$

where D_e is the equivolumetric spherical diameter, $N(D_e)$ the number of drops in $[D_e, D_e + dD_e]$ range, λ is the radar wavelength, and m the complex refractive index of the hydrometeors. The H and V polarization backscattering cross sections, $\sigma_{b\mathrm{H,V}}(D_e)$, and the forward, $f_{\mathrm{H,V}}(K_1, K_1; D_e)$, and backward, $f_{\mathrm{H,V}}(K_1, -K_1; D_e)$, scattering coefficients can be calculated for an assumed raindrop oblateness–size relation using the T-matrix method (Barber and Yeh 1975).

The above integral equations require selection of a raindrop oblateness–size relation. In this study we used a linear relationship between the raindrop's minor-to-major axis ratio (r_a) to its equivolumetric spherical diameter (D_e) (Matrosov et al. 2002):

$$r_a = (1.0 + 0.05\,\beta) - \beta\, D_e \quad \text{for} \quad D_e > 0.5 \text{ mm}, \tag{8}$$

where β is the slope of the shape–size relationship ($dr_a/d\ D_e$). The value 0.062 mm^{-1} approximated by Pruppacher and Beard (1970) for parameter β, brings Eq. (8) close to the equilibrium shape–size relation thereby denoted as the equilibrium shape parameter (β_e). There are numerous studies showing a varying degree of divergence from equilibrium condition, which is mainly attributed to drop oscillations and drop canting (Bringi et al. 2002; Keenan et al. 2001). In this study we evaluate the radar parameters for a number of β values and derived parameterizations that are β dependent. Selection of the optimal β value to be used in the retrieval will be discussed in the XPOL algorithm section.

Raindrop are assumed to follow a normalized gamma drop size distribution (Bringi and Chandrasekar 2002):

$$N(D) = N_W f(\mu)\left(\frac{D}{D_0}\right)^{\mu} e^{-(4+\mu)(D/D_0)} \ (\text{m}^{-3}\ \text{mm}^{-1}), \tag{9}$$

with

$$f(\mu) = \frac{6}{4^4}\frac{(4+\mu)^{(\mu+4)}}{\Gamma(\mu+4)}. \tag{10}$$

The above model has three parameters: the normalized intercept N_w, the median volume diameter D_0, and the shape parameter μ. Values for the three parameters are obtained on the basis of the 3-min-averaged raindrop spectra using a method similar to Bringi and Chandrasekar (2002). In short, the water content (W, in g m^{-3}) and the mass-weighted mean diameter (D_m, in mm) are calculated, based on which we obtain N_w (in mm^{-1} m^{-3}) as $N_w = (256/\pi)(1000W/D_m^4)$. The μ value is then estimated by minimizing the following least squares function:

$$\sum_x \left(\frac{N(x)}{N_w} - f(\mu)x^{\mu}\exp[-(4+\mu)x]\right)^2, \tag{11}$$

where summation is over discrete bins of normalized drop diameter ($x = D/D_m$) ranges and $N(x)$ is the relative frequency of measured spectra in bin $[x + dx]$.

The XPOL retrieval uses parameterizations that need to be evaluated on the basis of measured raindrop spectra. Consequently, for the triplets of DSD parameters fitted to measured DSD spectra we calculated rainfall rate and water content, while the corresponding XPOL parameters (Z_H, Z_{DR}, K_{DP}, A_H, A_{DP}, δ, etc.) were computed from the T-matrix method (Barber and Yeh 1975) assuming 1) the axis ratio of Eq. (8) for a range (0.032–0.092 mm^{-1}) of β values, 2) Gaussian drop canting angle distribution with zero mean and standard deviation 10, and 3) 6-mm maximum drop diameter. The raindrop dielectric constant of water droplets was evaluated at mean atmospheric temperatures of 25°C.

4. The XPOL algorithm for DSD parameter estimation

a. Algorithm formulation

Because of XPOL's short wavelength (~3 cm), the specific attenuation A_H and differential attenuation A_{DP} can be significant at moderate to high rainfall rates. The devised algorithm corrects for Z_H and Z_{DR} attenuation by evaluating the integral Eqs. (1) and (2) along a radar ray. For this purpose we use estimates of A_H and A_{DP} ray-path accumulations, which are derived from Ψ_{DP} profile as follows:

$$\int_0^r A_{\text{H}}(r)\,dr = \gamma(\beta) \times [\Psi_{\text{DP}}(r) - \Psi_{\text{DP}}(0)], \tag{12}$$

$$\int_0^r A_{\text{DP}}(r)\,dr = \varphi(\beta) \times \int_0^r A_{\text{H}}(r)\,dr. \tag{13}$$

The linear relationship assumed between specific attenuation (differential attenuation) and differential phase shift (specific attenuation) is a good approximation at X-band frequency. An important issue here is that γ and ϕ parameters are dependent on the selection of the axial ratio model's β value; consequently, the parameters were determined for different β values on the basis of the measured raindrop spectra, and are presented below

$$\gamma = 0.1454\beta^{-0.918}, \tag{14}$$

$$\phi = 0.145\beta^{0.122}. \tag{15}$$

The XPOL retrieval proceeds with estimating N_W and D_0 values for each radar bin along the ray. When the triplet of attenuation-corrected Z_H, Z_{DR}, and K_{DP} values, estimated from Ψ_{DP} profile, are greater than 25 dBZ, 0.3 dB, and 0.08° km^{-1}, respectively, we apply the

following experimental relationships derived from the measured raindrop spectra

$$\log_{10}(N_W) = A_1(\beta) + A_2(\beta)Z_H(\text{in dBZ}) + A_3(\beta)\log_{10}(K_{\text{DP}}), \quad (16)$$

$$D_0 = B_1(\beta)\left(\frac{Z_H}{N_W}\right)^{B_2(\beta)}. \quad (17)$$

The parameter sets ($A_{1,2,3}$ and $B_{1,2}$) are also dependent on β:

$$A_1 = 8.3202\beta^{-0.1541} \quad A_2 = -0.1294\beta^{0.1095} \quad (18)$$

$$A_3 = 1.8671\beta^{-0.0741} \quad B_1 = 1.5169\beta^{-0.0171} \quad (19)$$

$$B_2 = 0.123\beta^{-0.041}.$$

In all other cases, N_w value was fixed to the most frequent value derived from the raindrop spectra (i.e., 12 930 $\text{mm}^{-1}\ \text{m}^{-3}$), while D_0 was estimated from Eq. (17).

For a set of N_w and D_0 estimates we determine μ parameter by solving the constraining relation between μ and Λ defined as following (Brandes et al. 2003):

$$\mu = a\Lambda^2 + b\Lambda + c, \quad (20)$$

where

$$\Lambda = \frac{3.67 + \mu}{D_0}\,(\text{mm}). \quad (21)$$

Solving Eqs. (20) and (21) we end up solving a second-order equation of μ where we allow the solution that is physically acceptable (i.e., $-2 < \mu < 20$). The μ–Λ relation depends on D_0; consequently, the relationship parameters were determined here for different ranges of D_0 values: $D_0 \geq 2.0$ mm, $2.0 < D_0 \leq 1.5$, $1.5 < D_0 \leq 1.0$, and $D_0 < 1.0$. Those D_0 ranges were selected to minimize the scatter in μ–Λ relationship (not shown here), and give distinct (see Table 2) parameters values.

b. Selection of optimal β value

The XPOL algorithm used in attenuation correction and DSD parameter estimation depends on the selection of β parameter value. As shown in Anagnostou et al. (2004) a varying β value could significantly affect the determination of path-integrated attenuation and the estimation of DSD parameters. Matrosov et al. (2002) have proposed an estimator for β relating its value to the radar parameters (Z_H, Z_{DR}, and K_{DP}); a procedure similar to the one developed by Gorgucci et al. (2000) for S-band retrieval. Unfortunately, in contrary to what seen in the β estimator for S band, estimation of β at X band is associated with significant uncertainty. This is attributed to the wide scatter in the β–(Z_H, Z_{DR}, K_{DP}) relationship (see Fig. 2 in Matrosov et al. 2002), and to that the estimator uses attenuation-corrected Z_H and Z_{DR} parameters. The latter introduces an additional complication, as it requires solving the coupled problem of attenuation correction and β estimation in an iterative way. Sometimes under significant noise in the measurement, the solution from those iterations may lead to unphysical values. In this study, we devised a procedure to determine a single optimal value for β. The procedure selects the β values that offer the best consistency between XPOL attenuation-corrected Z_H and Z_{DR} parameters and the corresponding radar parameters calculated from raindrop spectra. The analysis showed that the best agreement between the measured and calculated Z_H–Z_{DR} relationship is achieved with $\beta = 0.055\ \text{mm}^{-1}$; consequently, this is the value selected for use in the XPOL retrieval. A recent study by Matrosov et al. (2005) has independently concluded on a similar optimal value ($0.057\ \text{mm}^{-1}$) for the β parameter.

TABLE 2. Parameters of $\mu-\Lambda$ relation for four different mean drop diameter ranges.

D_0	a	b	c
$D_0 \geq 2.0$	−3.5752	2.7225	−0.0751
$1.5 \leq D_0 < 2.0$	−3.5308	1.5542	0.020962
$1.0 \leq D_0 < 1.5$	−3.0334	1.277	−0.016033
$D_0 < 1.0$	−4.9745	1.2067	−0.015526

5. Results

a. Evaluation of attenuation correction

On 10 September 2001 a squall line formed on the northwest of XPOL (~30-km range) and north of the WSR-88D (~15-km range). The squall line remained well organized and within the coincident measurement area of the two radars for 1 h. The reflectivity values in the convective cores ranged between 45 and 53 dBZ causing notable attenuation in XPOL measurements. The stratiform portion of the storm was associated with less spatial variability, larger spatial extend, and reflectivity values ranging between 20 and 35 dBZ. Figure 3 shows a snapshot of coincident storm measurement by XPOL and 88D, along with the corresponding XPOL attenuation-corrected reflectivity field and retrieved N_w field. It is noted that at parts of the storm following major convective cores, attenuation correction increases the reflectivity values by as much as 10 dB. Comparison with the corresponding 88D reflectivity measurements shows that attenuation correction makes XPOL observations quantitatively consistent to 88D. The agreement between the two radar measurements is high. Figure 4 shows scatterplots of 88D versus XPOL

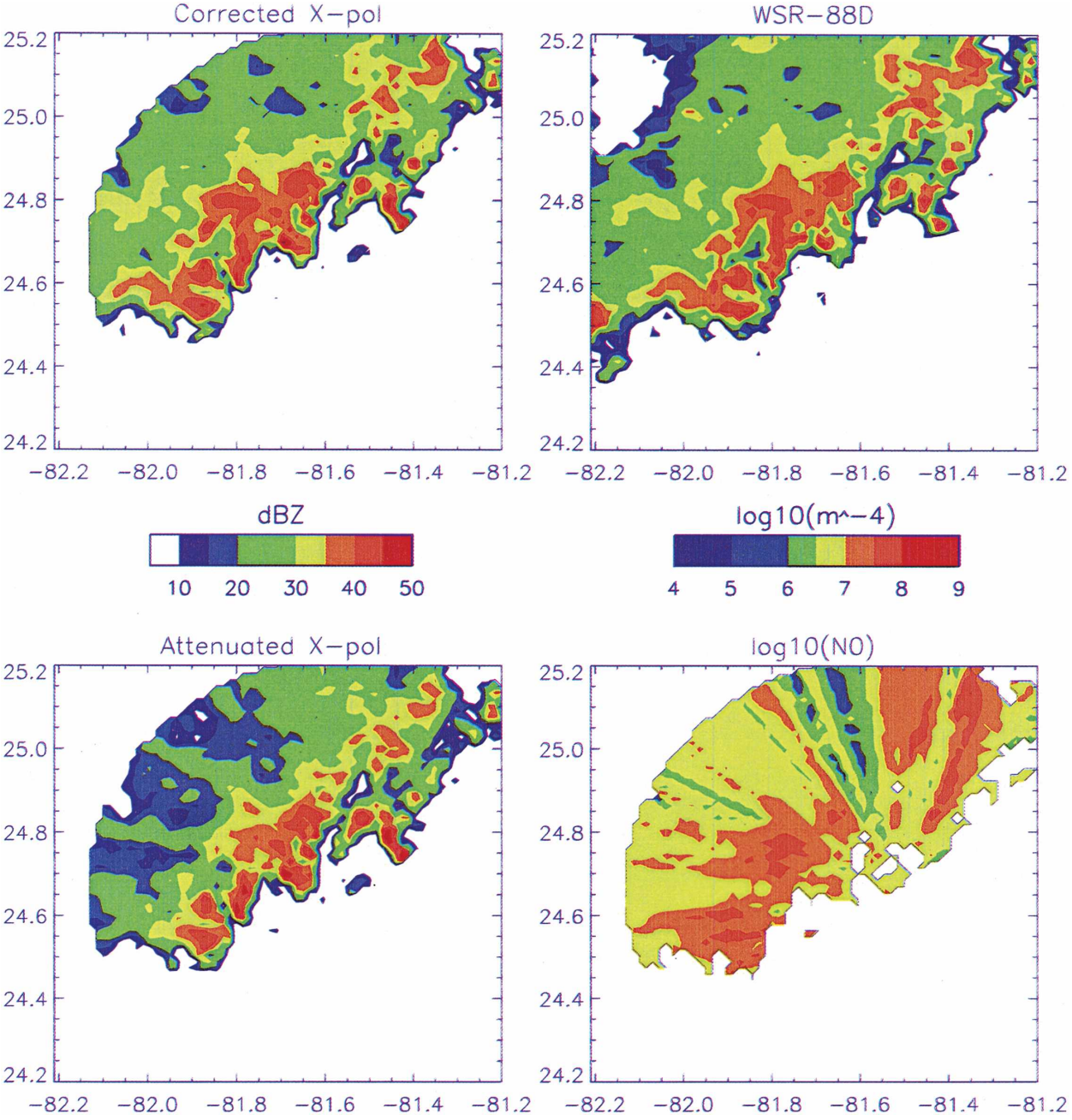

FIG. 3. (lower left) XPOL raw and (upper left) attenuation-corrected reflectivity fields, the corresponding (lower right) N_w retrieval field, and coincident reflectivity field from (upper right) the Key West WSR-88D. The measurement is from 10 Sep 2001 (1728 UTC).

reflectivity values derived from the whole storm period, before (left panel) and after (right panel) attenuation correction was applied to XPOL data. A first observation is that after correction XPOL reflectivity values become unbiased with respect to those of 88D. It is noted that 88D and XPOL reflectivities had been adjusted for the −1 and +3 dB calibration offsets, respectively. Excluding outliers the range of scatter between raw XPOL and 88D reflectivities is up to 30 dBZ, while in the case of attenuation-corrected XPOL data it does not exceed 15 dBZ. This is reflected on the correlation between XPOL and 88D, which increases from 0.73 in the case of raw XPOL data to 0.85 after attenuation correction is applied.

Results shown in Figs. 3 and 4 indicate that XPOL attenuation-corrected data can represent the variability

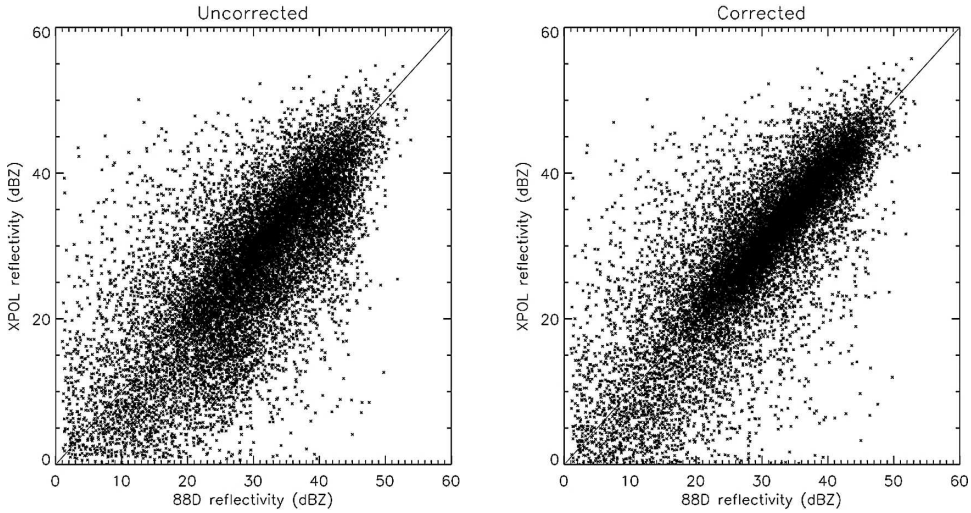

FIG. 4. Scatterplots of XPOL vs WSR-88D coincidental reflectivity values from the storm of 10 Sep 2001 (left) before and (right) after attenuation correction.

of convective precipitation as reliably as a nonattenuated S-band radar. This is an important observations, because as mentioned in the introduction, the attenuation correction in convective, or highly variable in space, precipitation, is challenging, as K_{DP} estimates are subject to error, due to potential δ effects, and measurement noise. Consequently, there is no guarantee that an attenuation correction procedure that works well in the low intensity stratiform precipitation would work as well in the case of intense convective rainfall systems. The results in this section suggest that the algorithm presented in this study performs reasonably well in convective precipitation. We analyzed various other cases consisting of organized systems or isolated cells and the results were similar. The results in this section, along with those on DSD and water content retrieval presented in the subsequent sections, may serve as an indication of the overall algorithm consistency.

b. Evaluation of DSD parameters retrieval

In this section we evaluate the estimation of the two main DSD parameters (N_w, D_0) through comparison of their frequency distributions against the corresponding parameters calculated from DSD measured spectra. Attenuation-corrected and offset-adjusted XPOL data from low elevation sweeps (0.5°–1.0°) of up to 30-km radar range were used in these statistics. Figure 5 shows the histograms of N_w and D_0 parameters, and Fig. 6 shows contour plots of the joint N_w–D_0 frequency determined from XPOL retrievals and the DSD-calculated dataset. The main observation from those plots is that the XPOL-retrieved DSD parameters are statistically consistent with the parameters calculated based on DSD data. The distributions are comparable in terms of the different statistics (mode, mean, variance). Specifically, the mode of XPOL log10(N_w) values is 3.4 compared to the 3.5 of the disdrometer calculations. Mean and variance differences between XPOL and disdrometer for log10(N_w) are within 0.2. In D_0 the difference in the modes is about 0.4 mm, while the differences in the mean and variances are within 0.2 mm. The joint frequency plots show similarities in terms of the slope between N_w and D_0. However, XPOL-retrieved values are associated with smoother contours, which is due to the larger number of XPOL data. The XPOL-estimated N_w values reach higher values at the lower end of D_0 values compared to corresponding disdrometer calculations. In the upper end ($D_0 > 2$) the agreement between XPOL and disdrometer is better. It is noted that the XPOL and DSD data are not from matched pairs; consequently, differences of the order shown in these plots are expectable.

The third parameter, μ, is evaluated by comparing the scatterplots of rain rate versus N_w (D_0) derived from XPOL-retrieved and DSD-calculated parameters. The value of μ is inherent in the rain-rate calculations; consequently, the above comparison offers an indirect consistency check for μ retrieval. Figure 7 shows the scatterplots. The observation we make about μ is along the line with our conclusion about N_w and D_0 retrievals. Statistics of the retrieved relationships are consistent with those derived from DSD calculations. A point to note is that XPOL retrievals exhibit a wider extent of D_0 values than the disdrometer, particularly for high

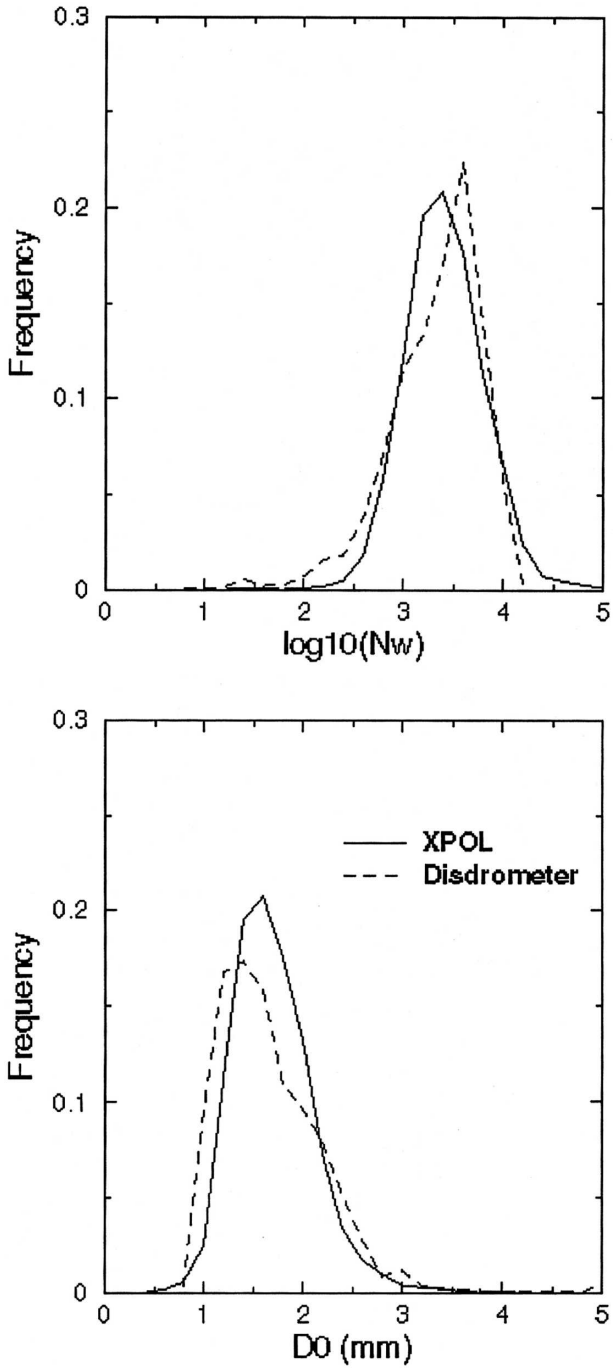

FIG. 5. Frequency histograms of $\log_{10}N_w$ (N_w in mm^{-1} m^{-3}) and D_0 (in mm) parameters calculated and retrieved from DSD and XPOL measurements, respectively.

rain rates. This could be due to the significantly larger number of XPOL data, noise in XPOL observations leading to errors in the DSD estimation, the sampling differences between the two instruments, and the fact that these are not coincident datasets. It is noted, however, that those scatterplots compare favorably with similar scatter plots derived by Bringi et al. (2002) on the basis of S-band polarimetric radar observations from the Large-Scale Biosphere–Atmosphere Experiment (LBA) in Amazonia (see Fig. 8 in Bringi et al.).

As a final point we present D_0 and N_w frequency plots (see Fig. 8) derived from XPOL data for two distinct precipitation scenarios, that is, convective rain rates with rainfall intensities greater than 30 mm h^{-1}, and a mixture of convective and stratiform rain rates with intensities between 0.5 and 10 mm h^{-1}. Quantitative results are summarized in Table 3, which presents the mean and standard deviation of D_0 and N_w parameters. We note that there is a higher concentration (or lower scatter) of both N_w and D_0 parameters in the low intensity rain rates. High rain rates are associated with statistically larger N_w values and larger D_0 tails. These conclusions are also drawn by the mean and standard deviation statistics shown in Table 3. The statistics of the N_w and D_0 parameters derived by XPOL in KAMP are similar to what presented by Bringi et al. (2002) on the basis of DSD parameters retrieved from S-band dual-polarization Doppler radar (S-Pol) observations in the western Amazon (LBA Experiment). We note, though, that the random deviations of the parameters retrieved in KAMP are systematically higher than what shown in the other studies. We speculate an explanation to this being that we have used a very large sample (about one month of storm data, or over 5×10^6 rainy pixels) to derive those statistics, while the other studies were concerned with smaller data samples (e.g., Bringi et al. selected their sample through visual inspection of the storm data). Another justification could be the larger variability in storm types exhibited during KAMP field experiment (we sampled a number of convective storms ranging from early morning isolated convective cells to organized squall lines with extended stratiform rain areas, e.g., 10 and 27 September).

c. Results from the 19 September KAMP flight mission

In KAMP, 19 September was a deployment day associated with coincident ground and airborne observations. A high-quality airborne dataset from that day is of precipitation profiles measured by ER-2 Doppler radar on board NASA's ER-2 high-altitude aircraft. EDOP is dual-beam 9.6-GHz radar used to measure the reflectivity and wind structure in precipitation systems. In this section we use EDOP profile observations from a flight leg (1808–1816 UTC) on 19 September that has

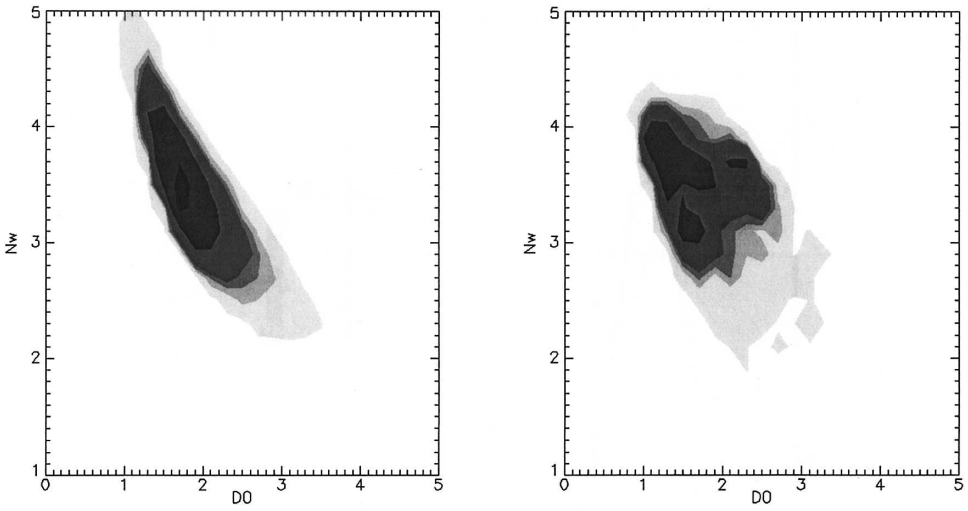

FIG. 6. Contour plots of joint frequency between $\log_{10}(N_w)$ and D_0 parameters (N_w in $\text{mm}^{-1}\ \text{m}^{-3}$ and D_0 in mm); (left) XPOL-retrieved and (right) DSD-calculated parameters.

close coincidence with XPOL observations. Unfortunately, the varying mission priorities within CAMEX, and weather conditions, did not allow us to collect more of such coincident datasets in KAMP. Shown on the top panel of Fig. 9 are the EDOP reflectivity profiles along the flight leg. These values are subject to rain-path attenuation. To correct for attenuation, we used the algorithm of Grecu and Anagnostou (2002). The attenuation-corrected reflectivity profiles are displayed in the middle panel of Fig. 9. The attenuation correction algorithm relies on independent information concerning the path-integrated attenuation (PIA). As shown in Grecu and Anagnostou (2002), this information can be determined from a surface return technique (SRT) or from passive radiometer observations. The PIA estimates from SRT and an analytical formulation (Hitschfeld and Bordan 1954) for PIA were conjointly used to correct for attenuation in EDOP reflectivity profile and to estimate N_w. The reader is referred to Grecu and Anagnostou (2002) for further details on the technique.

The accuracy in estimating N_w depends on the accuracy of determining PIA from SRT. SRT estimation of PIA requires large attenuation paths to minimize noise effects. At EDOP frequency (X band, 9.3 GHz) this can only occur in deep convective profiles. Consequently, estimation of N_w was only performed in parts of the flight leg associated with deep convection, which extend from −81.10° to about −80.80°W. Anywhere else, we used an N_w value considered in TRMM PR algorithm for convective rain (Ferreira et al. 2001). The PIA estimated by this algorithm (denoted as HB) and the one derived from SRT alone are shown at the lower

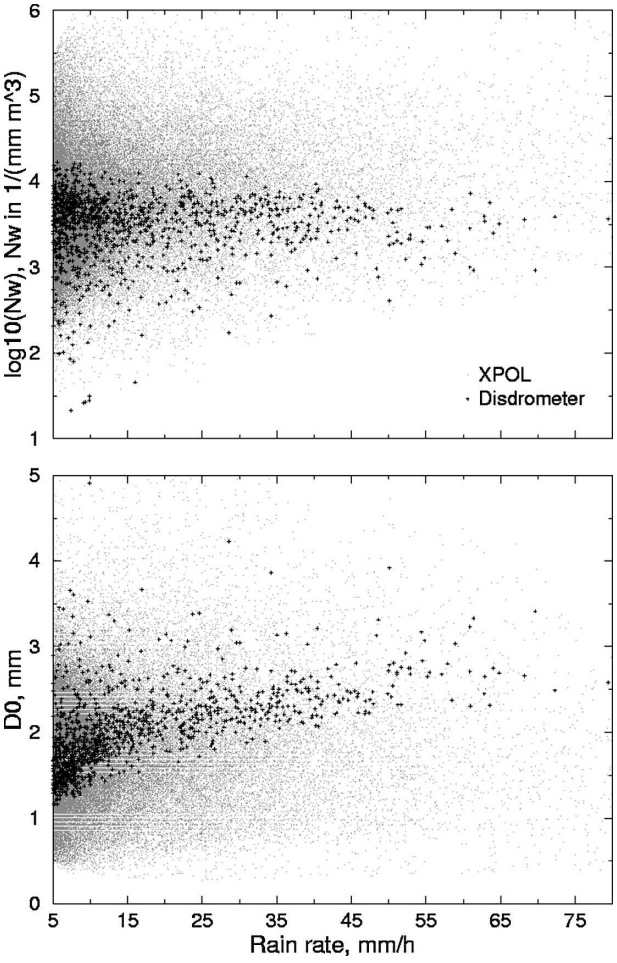

FIG. 7. Scatterplots of rain rate vs (top) $\log_{10}N_w$ and (bottom) D_0 derived from DSD parameters retrieved and calculated from XPOL and DSD measurements, respectively.

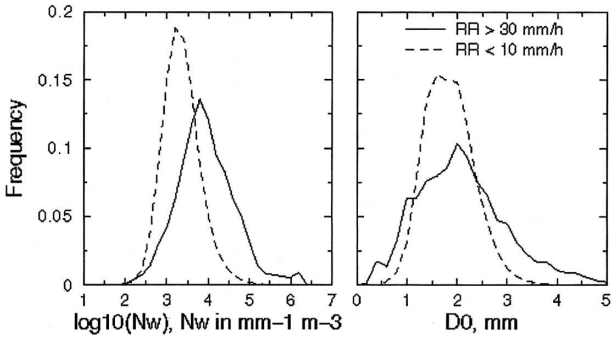

FIG. 8. Frequency histograms of XPOL retrieved N_w and D_0 parameters for two distinct rain-rate categories: RR > 30 mm h^{-1} and RR < 10 mm h^{-1}.

panel of Fig. 9. The agreement between HB and SRT PIA values is good in convective precipitation profiles where rain-path attenuation is large and associated with more reliable SRT calculations. At low rain-path attenuation profiles, SRT estimates of PIA are noisy; consequently, as noted above their differences with the HB analytical solution cannot be used to reliably determine deviations of N_w.

EDOP reflectivity and precipitation retrievals are next compared to XPOL data. In Fig. 10 we show EDOP attenuation-corrected reflectivity values versus raw (and attenuation corrected) XPOL reflectivity values projected on the EDOP flight leg. Matched data from four XPOL elevation sweeps (1.41°, 3.1°, 4.09°, and 6.14°) are presented here. We note a fairly good agreement between EDOP and the attenuation-corrected XPOL reflectivities. At all elevations, XPOL observations exhibit significant attenuation (about 20 dB at 1.41°, 30–40 dB at 3.1°, 15 dB at 4.09°, and 7 dB at 6.14°). The attenuation correction appears to be effective in most cases. For example, at 3.1° elevation the agreement between XPOL and EDOP values is within 2 dB in most parts of the deep convective cell. For the other elevations, the agreement is still high, although some discrepancies exist in the −81.00° to −80.08°W range along the path. This may be caused by time differences and spatial mismatches as well as by uncertainties in the attenuation correction of either set of observations. Nevertheless, the XPOL attenuation correction is shown to improve significantly the agreement between EDOP and XPOL reflectivity values. The correlation between matched XPOL and attenuation-corrected EDOP reflectivity values increases from 0.80 to 0.85 after attenuation correction on XPOL. Note that the XPOL data used in this comparison were adjusted for the 2-dB positive bias identified from previous comparisons with 88D and MIPS. We next compare water content and N_w estimates from the two platforms.

TABLE 3. Statistics of N_w and D_0 parameters derived from XPOL retrievals.

	RR > 30 mm h^{-1}	$0.5 \leq$ RR < 10 mm h^{-1}
$\log_{10}(N_w)$, N_w in mm^{-1} m^{-3} Mean (std dev)	4.3 (0.49)	3.4 (0.31)
D_0, in mm Mean (std dev)	1.74 (0.62)	1.81 (0.28)

Figure 11 shows EDOP and XPOL estimated water content values for the flight leg corresponding to Fig. 10. The correlation between XPOL and EDOP water content estimates is 0.87, with XPOL total water content being about 10% higher than the total water content estimated by EDOP observations. This difference originates from the slightly higher XPOL reflectivity values at longitudes west of −81°W. This is a region where XPOL and EDOP do not exhibit significant attenuation; thus, their reflectivity differences are mainly due to sampling mismatches (we particularly note the largely different scanning patterns of the two instrument) and differences in the observational times. Not correcting for attenuation leads XPOL estimating about half of the water content derived from EDOP observations, which again illustrates the impact of attenuation correction on the overall estimation.

In Fig. 12 we show comparison of EDOP and XPOL in terms of their N_w estimates. The N_w estimates from EDOP are available only within the deep convective structure, extending from −81.1° to −80.9°W, where such estimation is possible on the basis of SRT. It should be noted that only one value per vertical profile is estimated from EDOP observations, which is then matched to the corresponding XPOL values from the different elevation sweeps. There appears to be satisfactory agreement between the two N_w retrievals, considering that both estimates involve radial averaging and are subject to independent random errors in PIA. A common observation in both retrievals is that N_w increases within the convective core and that the range of values is consistent in the estimates from the two methods. The correlation between XPOL and EDOP N_w retrievals is 0.75. The average N_w values retrieved from XPOL and EDOP observations in the convective core are 7.51 and 7.33 [in $\log_{10}(\text{m}^{-4})$], respectively.

Although we do not claim that XPOL (or EDOP) retrievals are sufficiently certain to serve as validation for the other sensor retrievals, we consider that the above analysis lends credence to the XPOL algorithm and the data presented in the previous sections. As mentioned in the introduction, one major KAMP ob-

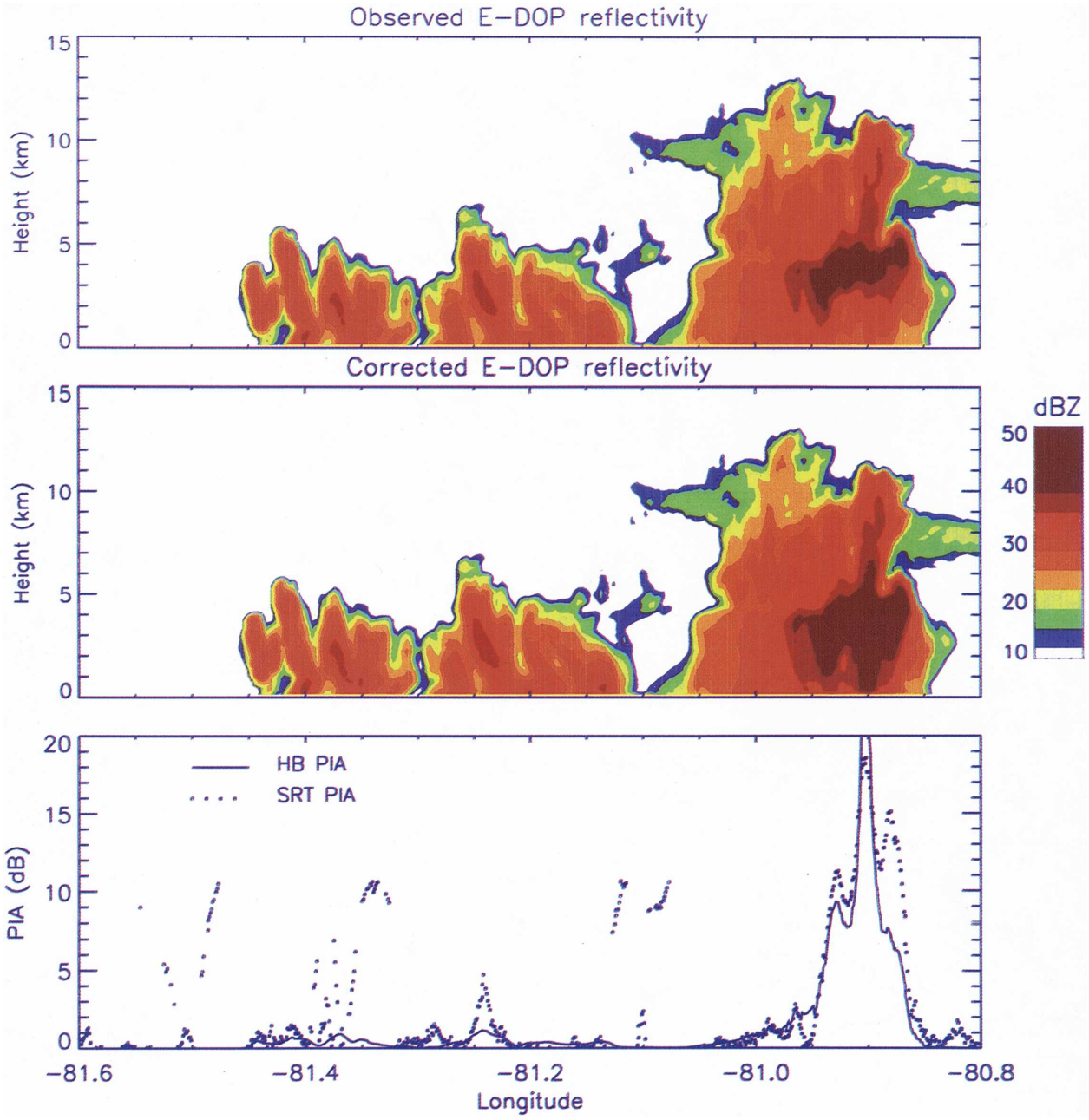

FIG. 9. (top) Observed and (middle) attenuation-corrected EDOP reflectivity profiles for a flight leg (1808–1816) on 19 Sep KAMP mission. (bottom) PIA estimates from Hitchfeld and Bordan (1954), HB, method, and the SRT.

jective resided in the collection of coincident data by various instruments to facilitate the refinement and validation of cloud-resolving models and satellite precipitation algorithms. The analysis presented in this paper intent to reinforce our statement that precipitation parameters derived from XPOL observations are consistent with those derived from other more contemporary sensor observations (such as those from disdrometer, airborne profiling radar, and high-power S-band polarimetric radar). The added advantage of XPOL observations in this case is its ability to provide high resolution three-dimensional observations required in the understanding of the dynamics of precipitation and its remote sensing from space.

6. Conclusions

An X-band dual-polarization and Doppler radar on wheels (XPOL) was deployed in KAMP as part of the

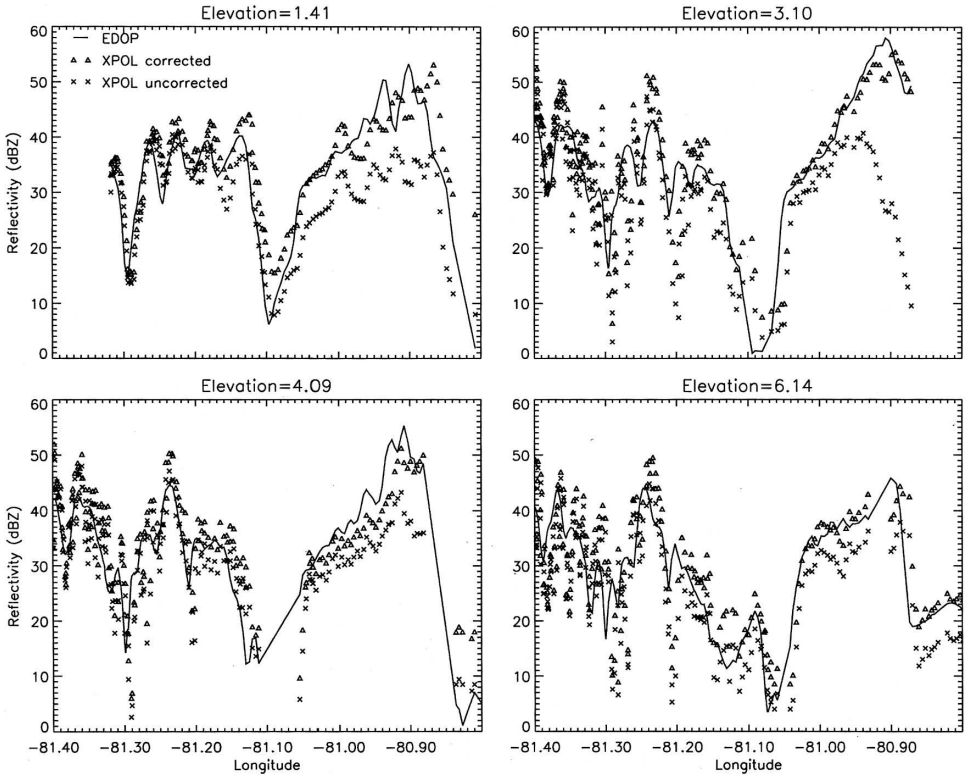

FIG. 10. Attenuation-corrected EDOP and XPOL (raw and attenuation corrected) reflectivity profiles matched along the EDOP flight leg. Each panel corresponds to a different XPOL elevation angle.

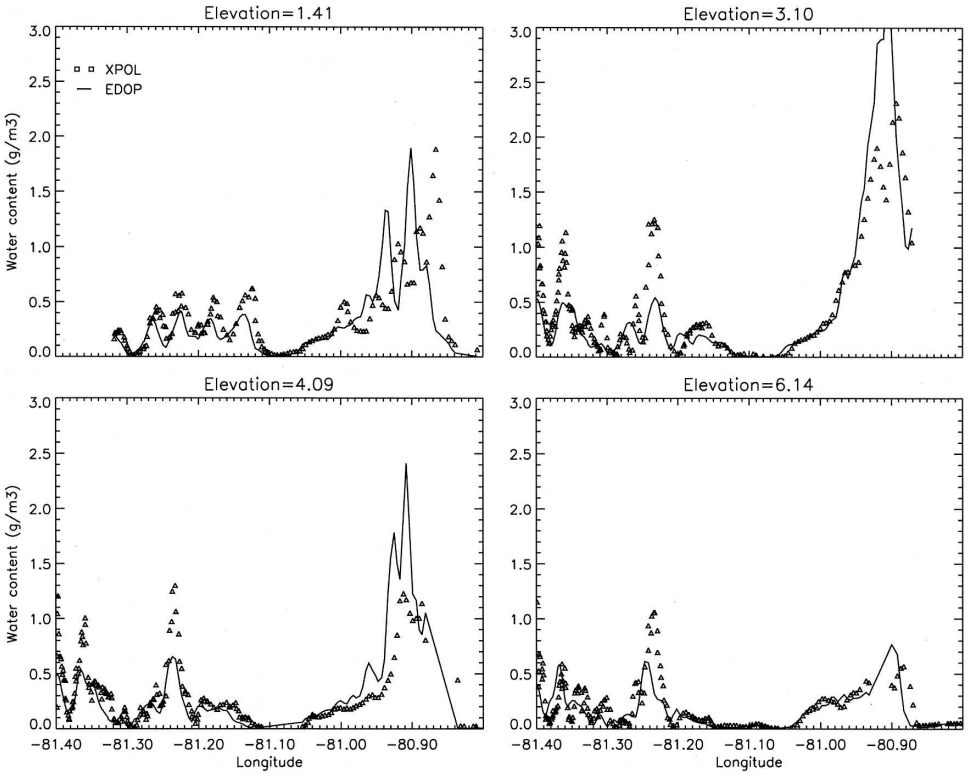

FIG. 11. Same as in Fig. 10, but for water content retrievals (g m^{-3}).

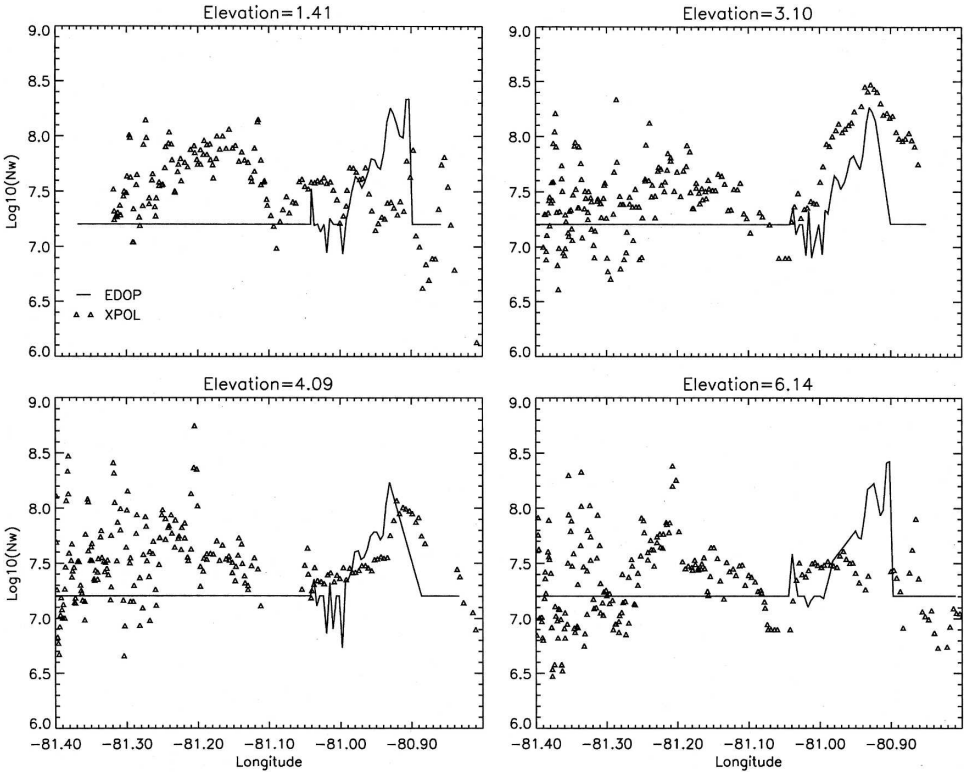

FIG. 12. Same as in Fig. 10, but for estimated $\log_{10}(N_w)$, where N_w is given in m^{-4}.

CAMEX field campaign. The XPOL deployment objectives were to provide high-resolution microphysical measurements of oceanic tropical rain systems. Combining those measurements with coincident wind retrievals from dual-Doppler radar data and other ground (disdrometers, gauges, and MIPS) and airborne measurements we aim at facilitating investigations on improving cloud-resolving model and radiometric simulations of tropical convection. This study was concerned with the XPOL measurements, calibration issues, and precipitation parameter estimation. The developed algorithm involved attenuation correction for reflectivity and differential reflectivity XPOL ray profiles, filtering the Φ_{DP} profile to remove noise, and the retrieval of the three parameters of the normalized gamma DSD model. The XPOL algorithm used parameterizations evaluated on the basis of measured raindrop spectra provided by NASA's TRMM office. The dependence of those algorithm parameters on oscillations of raindrop's oblateness–size relationship was investigated. An objective method was devised for selecting the most representative oblateness–size relation to be used in the retrieval.

The XPOL reflectivity measurements were found to have a positive bias of about 3 dB after attenuation correction with respect to the Key West 88D radar reflectivity measurements and MIPS profiler. The Z_{DR} measurements were moderately biased ($\sim$0.3 dB). Rain-path attenuation was shown to improve consistently the agreement between XPOL and different independent datasets. For example, comparison with 88D gave a correlation of 0.85, and comparison with EDOP correlation of 0.85. The DSD parameter retrieval results were statistically compared to corresponding DSD parameters calculated from the measured raindrop spectra. The statistical comparison showed that the retrieval offers DSD parameters that are consistent with in situ observations. XPOL-retrieved DSD parameter statistics were calculated for two rain-rate classes ($>$30 and $<$10 mm h^{-1}). The comparison showed differentiation in the parameter statistics, which agrees well with published results of Bringi et al. (2002).

The corrected for attenuation XPOL measurements and DSD parameter retrievals are now available for precipitation and remote sensing investigations. Unfortunately, KAMP did not achieve significant coincidence between airborne and ground-based observations. Nevertheless, on 19 September 2001, there were airborne measurements of convective cells occurring within XPOL's quantitative range. In this study we presented

a comparison between XPOL and EDOP measurements for one of the ER-2 flight legs on that date. Analysis showed good quantitative agreement (both in terms of systematic differences and correlation) between matched EDOP and XPOL water content and N_w estimates. Our overall assessment is that ground measurements from mobile experimental systems, such as XPOL, could provide datasets on precipitation parameters that are consistent to estimates derived from other more contemporary sensors (e.g., disdrometers, airborne and ground-based profiling systems, S-band polarimetric radars). Combining XPOL high resolution 4D (space and time) precipitation measurements with other in situ and remotely sensed observations we could achieve better understanding on precipitation microphysics and lead to improvements on precipitation remote sensing.

Acknowledgments. This research was cofunded by NASA–CAMEX project and NSF-CAREER award to Prof. E. N. Anagnostou. The quality controlled disdrometer dataset was provided by Dr. Ali Tokay of NASA TRMM office. The WSR-88D data were provided by Mr. David Wolf of NASA TRMM office. EDOP data were provided by Drs. Gerald Heymsfield and Lin Tian of NASA GSFC. TRMM PR data were provided by DAAC of the NASA Goddard Space Flight Center.

REFERENCES

Anagnostou, E. N., C. Morales, and T. Dinku, 2001: The use of TRMM precipitation radar observations in determining ground radar calibration biases. *J. Atmos. Oceanic Technol.,* **18,** 616–628.

——, M. N. Anagnostou, W. F. Krajewski, A. Kruger, and J. M. Benjamin, 2004: High-resolution rainfall estimation from X-band polarimetric radar measurements. *J. Hydrometeor.,* **5,** 110–128.

Barber, P., and C. Yeh, 1975: Scattering of electromagnetic waves by arbitrarily shaped dielectric bodies. *Appl. Opt.,* **14,** 2864–2872.

Blackman, T. M., and A. J. Illingworth, 1997: Examining the lower limit of KDP rain-rate estimation including a case study at S-band. Preprints, *28th Int. Conf. on Radar Meteorology*, Austin, TX, Amer. Meteor. Soc., 117–118.

Brandes, E. A., G. Zhang, and J. Vivekanandan, 2003: An evaluation of a drop distribution–based polarimetric radar rainfall estimator. *J. Appl. Meteor.,* **42,** 652–660.

Bringi, V. N., and V. Chandrasekar, 2002: *Polarimetric Doppler Weather Radar: Principles and Applications*. Cambridge University Press, 636 pp.

——, G.-J. Huang, V. Chandrasekar, and E. Gorgucci, 2002: A methodology for estimating the parameters of a gamma raindrop size distribution model from polarimetric radar data: Application to a squall-line event from the TRMM/Brazil campaign. *J. Atmos. Oceanic Technol.,* **19,** 633–645.

Chandrasekar, V., and V. N. Bringi, 1988a: Error structure of multiparameter radar and surface measurements of rainfall. Part I: Differential reflectivity. *J. Atmos. Oceanic Technol.,* **5,** 783–795.

——, and ——, 1988b: Error structure of multiparameter radar and surface measurements of rainfall. Part II: X-band attenuation. *J. Atmos. Oceanic Technol.,* **5,** 796–802.

——, ——, V. N. Balakrishnan, and D. S. Zrnic, 1990: Error structure of multiparameter radar and surface measurements of rainfall. Part III: Specific differential phase. *J. Atmos. Oceanic Technol.,* **7,** 621–629.

Ferreira, F., P. Amayenc, S. Oury, and J. Testud, 2001: Study and tests of improved rain estimates from the TRMM precipitation radar. *J. Appl. Meteor.,* **40,** 1878–1899.

Gorgucci, E., G. Scarchilli, and V. Chandrasekar, 2000: Practical aspects of radar rainfall estimation using specific differential propagation phase. *J. Appl. Meteor.,* **39,** 945–955.

Grecu, M., and E. N. Anagnostou, 2002: Use of passive microwave observations in a radar rainfall-profiling algorithm. *J. Appl. Meteor.,* **41,** 702–715.

Hitschfeld, W., and J. Bordan, 1954: Errors inherent in the radar measurement of rainfall at attenuating wavelengths. *J. Meteor.,* **11,** 58–67.

Hubbert, J. V., and V. N. Bringi, 1995: An iterative filtering technique for the analysis of coplanar differential phase and dual-frequency radar measurements. *J. Atmos. Oceanic Technol.,* **12,** 643–648.

Jameson, A. R., 1991: A comparison of microwave techniques for measuring rainfall. *J. Appl. Meteor.,* **30,** 32–54.

——, 1994: An alternative approach to estimating rainfall rate by radar using propagation differential phase shift. *J. Atmos. Oceanic Technol.,* **11,** 122–131.

Joss, J., and A. Waldvogel, 1967: A raindrop spectrograph with automatic analysis. *Pure Appl. Geophys.,* **68,** 240–246.

Keenan, T. D., L. D. Carey, D. S. Zrnić, and P. T. May, 2001: Sensitivity of 5-cm wavelength polarimetric radar variables to raindrop axial ratio and drop size distribution. *J. Appl. Meteor.,* **40,** 526–545.

Kummerow, C., and L. Giglio, 1994: A passive microwave technique for estimating rainfall and vertical structure information from space. Part I: Algorithm description. *J. Appl. Meteor.,* **33,** 3–18.

Matrosov, S. Y., R. A. Kropfli, R. F. Reinking, and B. E. Martner, 1999: Prospects for measuring rainfall using propagation differential phase in X- and Ka-radar bands. *J. Appl. Meteor.,* **38,** 766–776.

——, K. A. Clark, B. E. Martner, and A. Tokay, 2002: X-band polarimetric radar measurements of rainfall. *J. Appl. Meteor.,* **41,** 941–952.

——, D. E. Kingsmill, B. E. Martner, and F. Martin Ralph, 2005: The utility of X-band polarimetric radar for continuous quantitative estimates of rainfall parameters. *J. Hydrometeor.,* **6**, 248–262.

May, P. T., T. D. Keenan, D. S. Zrnić, L. D. Carey, and S. A. Rutledge, 1999: Polarimetric radar measurements of tropical rain at a 5-cm wavelength. *J. Appl. Meteor.,* **38,** 750–765.

Olson, W. S., C. Kummerow, G. M. Heymsfield, and L. Giglio, 1996: A method for combined passive–active microwave retrievals of cloud and precipitation profiles. *J. Appl. Meteor.,* **35,** 1763–1789.

Pruppacher, H. R., and K. V. Beard, 1970: A wind tunnel investigation of the internal circulation and shape of water drops falling at terminal velocity in air. *Quart. J. Roy. Meteor. Soc.,* **96,** 247–256.

Ryzhkov, A. V., and D. S. Zrnić, 1995: Comparison of dual-polarization radar estimators of rain. *J. Atmos. Oceanic Technol.,* **12,** 249–256.

Smith, A. H., R. W. Saunders, and A. M. Závody, 1994: The validation of ATSR using aircraft radiometer data over the tropical Atlantic. *J. Atmos. Oceanic Technol.,* **11,** 789–800.

Testud, J., E. Le Bouar, E. Obligis, and M. Ali-Mehenni, 2000: The rain profiling algorithm applied to polarimetric weather radar. *J. Atmos. Oceanic Technol.,* **17,** 332–356.

Tokay, A., D. B. Wolff, K. R. Wolff, and P. Bashor, 2003: Rain gauge and disdrometer measurements during the Keys Area Microphysics Project (KAMP). *J. Atmos. Oceanic Technol.,* **20,** 1460–1477.

Vivekanandan, J., D. N. Yates, and E. A. Brandes, 1999: The influence of terrain on rainfall estimates from radar reflectivity and specific propagation phase observations. *J. Atmos. Oceanic Technol.,* **16,** 837–845.

Walters, J. T., D.-K. Kim, K. R. Knupp, C. R. Williams, E. N. Anagnostou, and A. Tokay, 2004: Intercomparison of polarimetric radar, profiler and disdrometer observations of tropical precipitation during CAMEX-4/KAMP. Preprints, *26th Conf. on Hurricanes and Tropical Precipitation*, Miami, FL, Amer. Meteor. Soc., CD-ROM, 6A.2.

Zrnić, D. S., and A. V. Ryzhkov, 1996: Advantages of rain measurements using specific differential phase. *J. Atmos. Oceanic Technol.,* **13,** 454–464.

——, T. D. Keenan, L. D. Carey, and P. May, 2000: Sensitivity analysis of polarimetric variables at a 5-cm wavelength in rain. *J. Appl. Meteor.,* **39,** 1514–1526.